Sobhkhiz-Miandehi *et al.*
Earth, Planets and Space (2022) 74:88
https://doi.org/10.1186/s40623-022-01637-y

Earth, Planets and Space

FULL PAPER

Open Access

Comparison of the tidal signatures in sporadic E and vertical ion convergence rate, using FORMOSAT-3/COSMIC radio occultation observations and GAIA model

Sahar Sobhkhiz-Miandehi[1*], Yosuke Yamazaki[2], Christina Arras[2], Yasunobu Miyoshi[3] and Hiroyuki Shinagawa[4]

Abstract

Sporadic E or Es is a transient phenomenon where thin layers of enhanced electron density appear in the ionospheric E region (90–120 km altitude). The neutral wind shear caused by atmospheric tides can lead ions to converge vertically at E-region heights and form the Es layer. This research aims to determine the role of atmospheric solar and lunar tides in Es occurrence. For this purpose, radio occultation data of FORMOSAT-3/COSMIC have been used, which provide complete global coverage of Es events. Moreover, GAIA model simulations have been employed to evaluate the vertical ion convergence induced by solar tides. The results show both migrating and non-migrating solar tidal signatures and the semidiurnal migrating lunar tidal signature mainly in low and mid-latitude Es occurrence. The seasonal variation of the migrating solar tidal components of Es is in good agreement with those in the vertical ion convergence derived from GAIA at higher altitudes. Furthermore, some non-migrating components of solar tides, including semidiurnal westward wavenumbers 1 and 3 and diurnal eastward wavenumbers 2 and 3, also significantly affect the Es occurrence rate.

Keywords Sporadic E, Es, Wind shear, Solar tide, Lunar tide, GAIA, Radio occultation

*Correspondence:
Sahar Sobhkhiz-Miandehi
sahar@gfz-potsdam.de
Full list of author information is available at the end of the article

Graphical Abstract

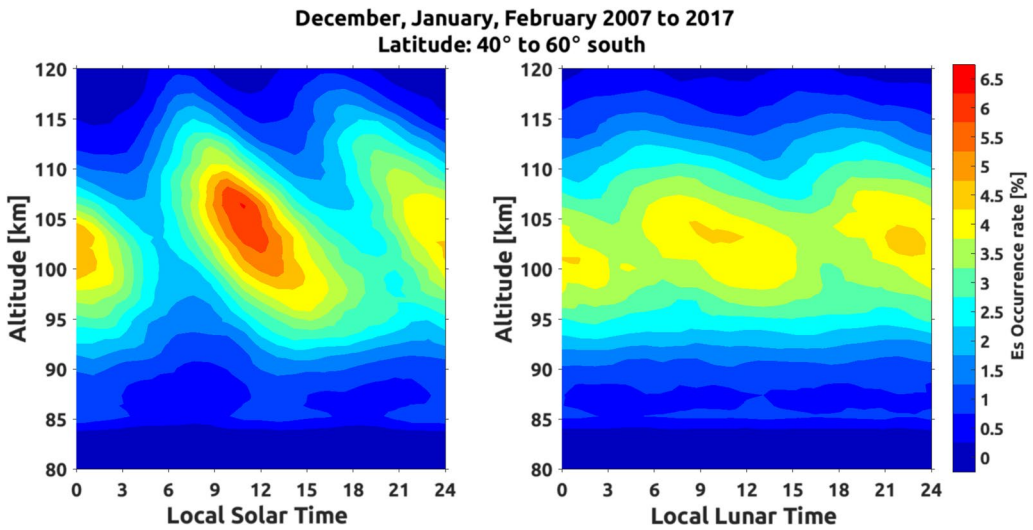

Introduction

Thin layers of enhanced electron density, which are detected in the lower thermosphere at the altitude range of 90 to 120 km, are referred to as Sporadic E and abbreviated as Es (Haldoupis 2011; Mathews 1998; Whitehead 1989). This transient phenomenon frequently occurs at mid- and low latitudes (Christakis et al. 2009; Haldoupis 2012; Haldoupis et al. 2007), mainly during the daytime in the summer hemisphere (Arras et al. 2010). Es layers have been the subject of many studies since the mid-twentieth century (e.g., Macleod 1966; Whitehead 1961, 1970, 1989) due to their impact on radio wave propagation in communication and navigation systems.

Wind shear theory is the most commonly accepted physical mechanism for mid-latitude Es layer formation (Haldoupis and Pancheva 2002; Haldoupis 2011; Yamazaki et al. 2022). According to wind shear theory, metallic ions such as Fe^+, Na^+, and Ca^+ in the ionosphere dynamo region, influenced by vertical shears of horizontal wind and the Earth's magnetic field, will converge vertically to a thin layer of ionization (Axford and Cunnold 1966; Haldoupis 2011).

At low/mid-latitudes, the wind shears in the lower thermosphere are mainly produced by atmospheric tides, including solar/lunar tides with the period of a solar/lunar day and its harmonics. Solar tides are known to be the primary source of vertical shears in the neutral wind at low/mid-latitude (Haldoupis 2012); hence a solar tidal signature is expected to be seen in the Es occurrence. Numerous studies have focused on the solar tidal signature in the Es layer. For example, Mathews and Bekeny (1979) demonstrated that the vertical motion of Es layers is consistent with diurnal and semidiurnal tides in the neutral atmosphere. Arras et al. (2009) presented semidiurnal solar tidal signatures in Es occurrence rate (EsOR) at northern hemisphere mid-latitude (50 °–55 N°). They compared EsOR with meteor radar wind measurements and found a strong relationship between semidiurnal tides in EsOR and vertical shear of zonal wind. Christakis et al. (2009) studied the mid-latitude Es layer seasonal variation and indicated diurnal tide influence on Es at altitudes below 110 km and semidiurnal tide dominance above that altitude. Oikonomou et al. (2014) also showed that a semidiurnal tide-like periodicity dominates Es layers. Terdiurnal and quarterdiurnal tidal signatures in Es occurrence rate are also indicated in other publications (e.g., Haldoupis and Pancheva, 2006; Fytterer et al. 2013; Jacobi et al. 2019). Recently, Liu et al. (2021) revealed a wavenumber 4 pattern in Es occurrence rate at mid and low latitudes formed by eastward propagating non-migrating diurnal tide with zonal wavenumber 3, and a similar feature was detected in the vertical shear of the zonal wind.

Shinagawa et al. (2017) calculated the vertical ion convergence rate using GAIA (Ground-to-topside model of Atmosphere and Ionosphere for Aeronomy) simulations to show how the geographical and seasonal variations of wind shears are consistent with those in EsOR. Andoh et al. (2020) simulated day-to-day variability of Es at mid-latitudes, using a numerical model driven by GAIA winds. Some previous studies have utilized GPS radio occultation (RO) measurements and combined them

with winds from different models such as HWM07 (Horizontal Wind Model 2007; Emmert et al. 2008), WACCM (the Whole Atmosphere Community Climate Model), and GAIA, to show neutral wind shear correspondence with Es (e.g., Chu et al. 2014; Liu et al. 2018; Qiu et al. 2019; Yeh et al. 2014). However, these studies did not address the relative importance of different migrating and non-migrating tides for Es layer formation and its seasonal dependence. This paper provides a tidal spectrum of Es occurrence rate using GPS radio occultation measurements and then compares them with tidal spectra of vertical ion convergence rate using GAIA model simulations which include both migrating and non-migrating tidal components.

Some investigations have been done on the lunar tide influences on Es using ground-based observations (e.g., Matsushita 1952, 1957, 1967; Stening 1999; Tarpley and Matsushita 1971, 1972), but none of them have provided a global picture of lunar tidal signature in the Es occurrence. The present study will look over global lunar tidal variations of Es occurrence using GPS radio occultation measurements.

Apart from atmospheric tides, planetary waves can also contribute to wind shear formation in the lower thermosphere. Some studies have suggested planetary wave effects on Es events (e.g., Haldoupis and Pancheva 2002; Pancheva et al. 2003; Haldoupis et al. 2004; Voiculescu et al. 1999), but planetary waves are not in the scope of the current paper. Interested readers can refer to the articles mentioned above.

FORMOSAT-3/COSMIC radio occultation data

For many years, Es events were mainly observed by ionosonde and sometimes in situ techniques (Mathews 1998; Matsushita 1962; Whitehead 1989). In the past two decades, many studies have benefited from the new GPS radio occultation methodology to obtain the global distribution of Es layers (Arras et al. 2008; Igarashi et al. 2001; Wu et al. 2005).

GPS radio occultation is a satellite remote sensing technique in which GPS signals are received by a low earth-orbiting satellite (LEO) after traveling through the atmosphere. Due to the atmospheric refractive index, the signals are bent on their way. This bending angle is the key observation to obtain information of the ionosphere and neutral atmosphere (Arras et al. 2010).

FORMOSAT-3/COSMIC (FORMOsa SATellite mission–3/Constellation Observing System for Meteorology, Ionosphere and Climate) consists of six LEO satellites, launched on April 2006. At the altitude of 80 to 130 km, scintillations are observed in SNR and phase measurements of FORMOSAT-3/COSMIC radio occultation signals, usually caused by Es layers. Signal phase differences, ionospheric excess phase, and SNR values are used in different literature to extract Es events from GPS-RO measurements (Igarashi et al. 2001; Wu et al. 2005). EsOR in this study is derived from the signal-to-noise ratio (SNR) profiles of GPS L1 signal of the level 1b atmPhs data product. Limiting thresholds has been set empirically to SNR values, and Es is defined as scintillations with SNR standard deviation more than 0.2 in a narrow altitude range. The method details can be found in Arras and Wickert (2018). Our investigations are based on FORMOSAT-3/COSMIC radio occultation data of the years 2007 to 2017.

GAIA model simulation data analysis

GAIA is a whole atmosphere model that has been developed by coupling three existing models**:** a whole atmosphere general circulation model (GCM) for deriving atmospheric neutral density, velocity, and temperature; an ionospheric model for ion density, ion, and electron temperature, and electric conductivity; and an electrodynamics model for the electric field (Jin et al. 2011). In the present study, the temperature and composition of the neutral atmosphere and the neutral wind velocity are obtained from the GAIA model with a grid spacing of 2.8 ° longitude by 2.8 ° latitude, 0.2 scale height, and a time resolution of 1 h. We have used reanalysis data-driven GAIA model simulation of the years 2007 to 2017. The model setup is basically the same as that used in Liu et al. (2017) and Miyoshi et al. (2017), but the simulation was extended to the year 2017.

Neglecting diffusion, electric field force, and vertical component of neutral wind velocity, the vertical ion drift velocity w_i can be written as follows (Mathews 1998):

$$w_i = \frac{r\cos I}{1+r^2}U + \frac{\cos I \sin I}{1+r^2}V, \tag{1}$$

where I is the Earth's magnetic field dip angle, U and V are magnetic eastward and southward neutral wind velocity, and r is the ratio of the ion-neutral collision frequency to the ion gyrofrequency. In the lower E region (90–115 km altitude), $r >> 1$ (Richmond 1995). Therefore, the zonal wind component is more efficient than the meridional wind component in causing vertical ion motion and, as a result, the Es layer formation (Haldoupis 2012).

Using geographical neutral wind velocities, U and V used in Eq. (1) are expressed as follows (Qiu et al., 2019):

$$\begin{cases} U = U' \cos D - V' \sin D \\ V = V' \cos D + U' \sin D \end{cases}, \tag{2}$$

where U' and V' are zonal and meridional wind velocities, respectively. U' and V' are derived from the GAIA

model, and D is the Earth's magnetic field declination angle, derived from International Geomagnetic Reference Field (IGRF; Finlay et al. 2010). We calculate the average vertical ion convergence rate (VIC) and assume only positive VICs lead to Es layer formation. Therefore, we can write VIC as (Shinagawa et al. 2017):

$$\mathrm{VIC} = \begin{cases} -\frac{\partial w_i}{\partial z}, -\frac{\partial w_i}{\partial z} > 0 \\ 0, -\frac{\partial w_i}{\partial z} < 0 \end{cases}. \quad (3)$$

Results

Es occurrence rate analysis

The Es occurrence rate is maximum in mid-latitude summer hemispheres (Arras et al. 2008), and in the latitude range of 40 ° to 60 ° south and north, tidal signatures are clearly seen. Therefore, we have analyzed two local summer periods of FORMOSAT-3/COSMIC radio occultation data: one is for the period of June, July, and August of years 2007 to 2017 at the latitude range of 40 ° to 60 ° north, and the other is December, January, and February of years 2007 to 2017 at the latitude range of 40 ° to 60 ° south. Binning the data into 1-km altitude by 1-h local time grids, altitude–local time cross-sections of the EsOR for the northern hemisphere summer is presented in Fig. 1. Maximum values of EsOR reach up to 13% in northern hemisphere summer.

A descending structure of EsOR with local solar time (LST) and local lunar time (LLT) is visible. EsOR variations with LST and LLT reveal a semidiurnal pattern at about 95–115 km altitude. The same applies to southern hemisphere summer shown in Fig. 2. However, the maximum values of EsOR reach only 6.5% in the southern hemisphere, which is almost half of that in the northern hemisphere. This can be due to South Atlantic Anomaly (SAA) region in which EsOR is significantly reduced (Arras 2010). Another possible explanation is that metallic ion density distribution might be different in southern hemisphere and northern hemisphere (Chu et al. 2014).

Tidal modulations at periods of 12 h are identified in the EsOR, with the peaks around 9 and 21 local time in the northern hemisphere. This confirms previous studies on solar and lunar tidal signature detection in northern hemisphere Es layers (e.g., Matsushita 1962; Arras et al. 2009). The phase of solar and lunar tidal signatures are slightly shifted in southern hemisphere EsOR. We have checked the lunar tidal variation at different local solar time and noted a consistent semidiurnal pattern (see Appendix 1).

Spatio-temporal characteristics of EsOR can be quantified using the least-square fitting method. This method estimates the amplitude and phase of tides at a specific frequency and zonal wavenumber, which enables us to separate migrating and non-migrating tidal components. We map the data in the frequency–wavenumber domain, and EsOR measurements can be expressed as:

$$\mathrm{EsOR} = \sum_{n,s} \{A(n,s)\cos[2\pi(nt + s\lambda)] + B(n,s)\sin[2\pi(nt + s\lambda)]\}, \quad (4)$$

where n is frequency, s is the zonal wavenumber, t is the normalized time of the day, and λ is the normalized longitude (Lühr and Manoj, 2013). In order to examine tidal components in EsOR, we have limited the data to the altitude range of 95–115 km, in which the solar and

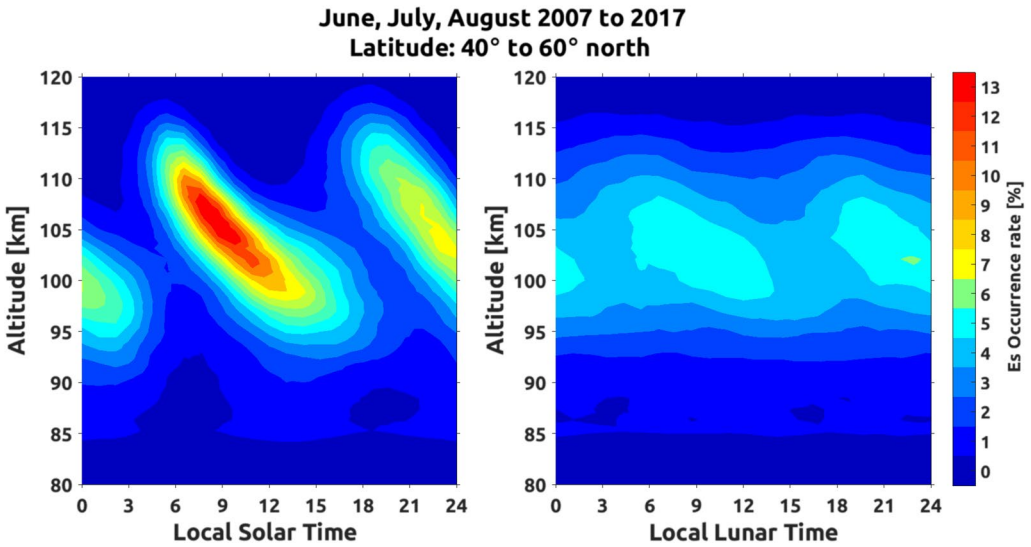

Fig. 1 Mid-latitude EsOR variations during northern hemisphere summer with solar local time (left) and lunar local time (right) at different altitudes

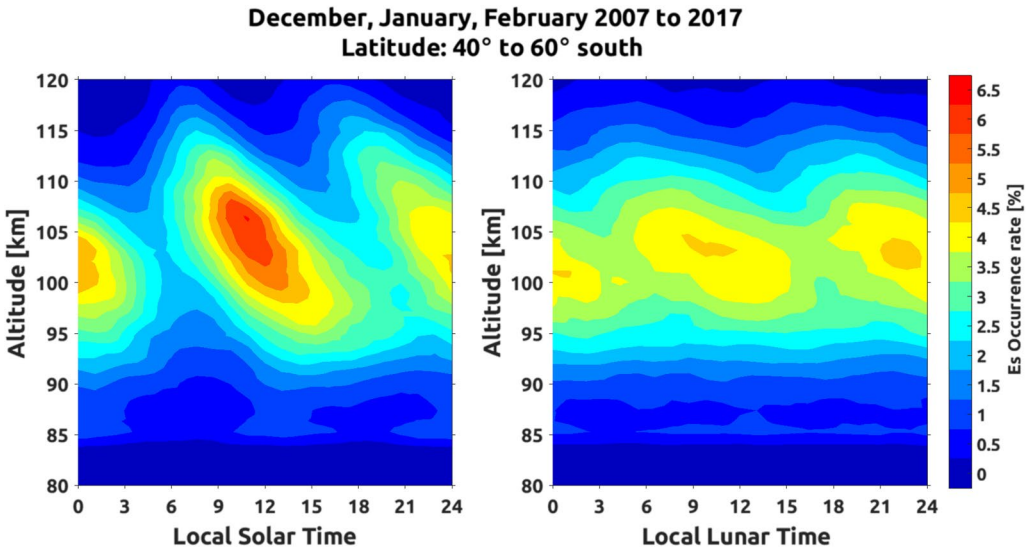

Fig. 2 Mid-latitude EsOR variations during southern hemisphere summer with solar local time (left) and lunar local time (right) at different altitudes

lunar tidal signatures are dominant, and binned them in 10 ° longitude by 1-h local time grids irrespective of the exact altitude between 95 to 115 km. Afterward, frequency–wavenumber analysis have been performed on the data similar to the method suggested in Lühr and Manoj (2013). Tides with the periods of 24 h, 12 h, 8 h, 6 h, respectively, are represented by n = 1, 2, 3, 4 and are referred to as diurnal, semidiurnal, terdiurnal, and quarterdiurnal tides (Forbes et al. 2008).

To describe different tidal components, we use the following terminology: tidal periods are represented by D, S, T, and Q, which are, respectively, corresponding to diurnal, semidiurnal, terdiurnal, and quarterdiurnal tides. Eastward (s < 0) and westward (s > 0) propagating tides are represented by E and W. These two letters are followed by an integer representing the zonal wavenumber. For example, DW1 means diurnal westward wavenumber 1, SE2 means semidiurnal eastward wavenumber 2, etc. The standing components are denoted as D0, S0, T0, and Q0.

The tidal spectra shown in Fig. 3 correspond to the amplitude of solar tides during local summers in northern and southern mid-latitudes. Different migrating and non-migrating tidal components are seen, among which the SW2 component has the highest amplitude in both summer hemispheres. For the northern hemisphere, DW1 is in second place; however, for the southern hemisphere, D0 is the second component with a high

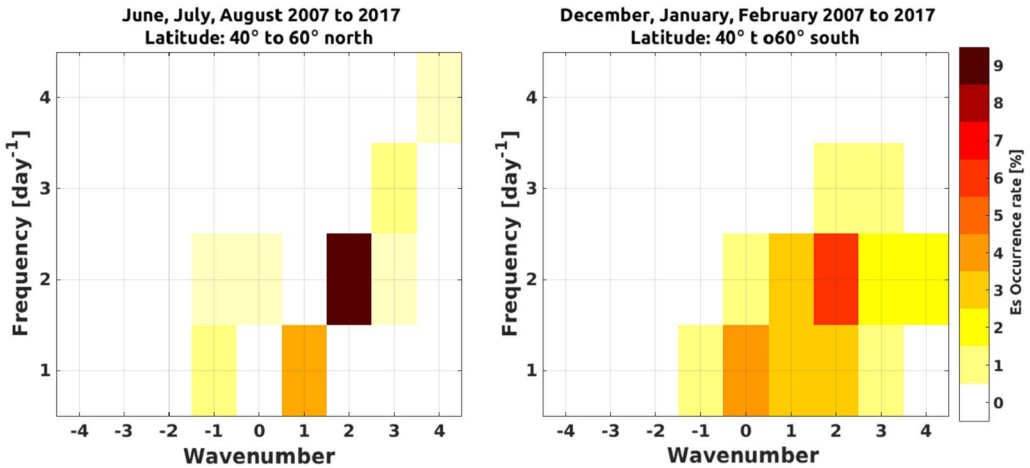

Fig. 3 Solar tidal spectra of mid-latitude EsOR amplitude during northern hemisphere summer (left) and southern hemisphere summer (right)

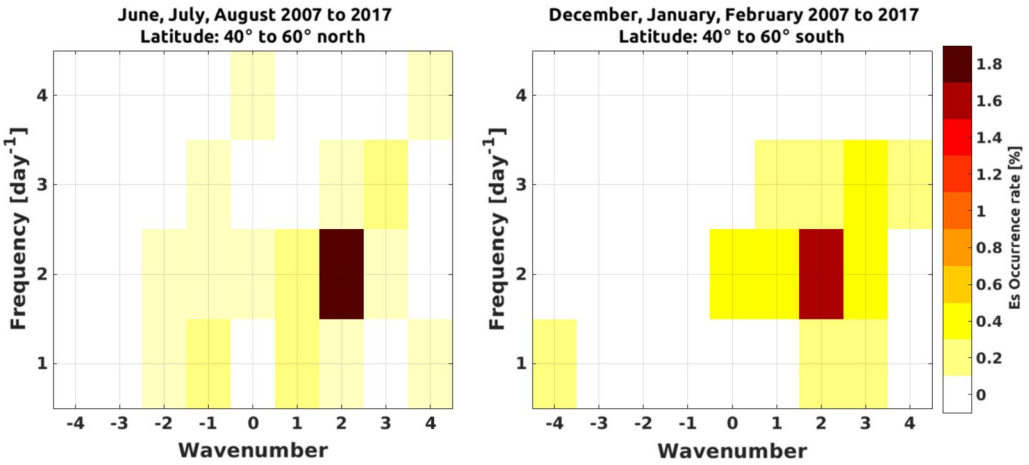

Fig. 4 Lunar tidal spectra of mid-latitude EsOR during northern hemisphere summer (left) and southern hemisphere summer (right)

amplitude. Figure 4 shows the tidal spectra of lunar tides signature in EsOR. Unlike solar tides, lunar tidal spectra show that only SW2 component is dominant in the summer hemispheres, and other tidal components are relatively small.

Comparison of VIC and EsOR

In order to compare tidal components of VIC and EsOR, tidal analysis has been performed on 11-year VIC and EsOR data sampled around 100, 105, 110, 115 km altitude. We studied the latitudinal variation of different tidal components of VIC and EsOR on a month-to-month basis at different altitudes. By calculating the correlation coefficients between each tidal component of VIC and EsOR at different altitudes, we realized that the altitude in which EsOR and VIC have the best correlation, vary for each component. For example, Fig. 5 reveals DW1 component of EsOR and VIC over different months and latitude bands at different altitudes. The seasonal variation of DW1 component of EsOR in different latitudes at 105 ± 5 km seems more similar to that of VIC at 110 and 115 km altitude than at 105 km. The correlation coefficient between DW1 in EsOR at 100 ± 5 km and VIC at 100 km is 0.16, while it reaches up to 0.73 when EsOR at 105 ± 5 km and VIC at 115 km are taken into account. We note that in general a tidal component of EsOR at a fixed altitude tends to correlate with the same tidal component of VIC at a.

higher altitude. Also the altitudes at which VIC and EsOR tidal components correlate the best, differ for different tidal components. This might be due to some inaccuracies in the tides of GAIA model simulations. However, this hypothesis still needs to be verified through comparisons of GAIA winds and neutral wind observations.

Four different migrating and non-migrating components of EsOR tidal spectra with the largest amplitude were determined, and their annual variations in different latitudes are displayed in Figs. 6 and 7. In addition, a comparison to the corresponding VIC tidal spectra at the altitude at which they have the best correlation with each other is made in those figures. Please note that at the magnetic equator, wind shear mechanism is not effective in Es layer formation and this needs to be taken into account when comparing EsOR and VIC in Figs. 6 and 7.

Among all migrating components of EsOR and VIC tidal spectra, SW2 has the highest amplitude. SW2 component of northern hemisphere VIC is present in all seasons, and it is dominant in mid-latitude local summers for EsOR and VIC. DW1 is the second, regarding its amplitude which is present throughout the year around the latitude band of 50 ° south to 50 ° north. Subsequently, TW3 and QW4 have lower amplitudes. Although month-to-month and latitudinal variations of SW2 and DW1 components of EsOR are in good agreement with those in VIC, seasonal variation of QW4 in EsOR is better consistent with VIC in the northern hemisphere rather than southern hemisphere; and TW3 component in EsOR is not necessarily similar to that in VIC from GAIA.

According to Fig. 7, at high and mid-latitudes, SW1 has the largest amplitude among all non-migrating components of EsOR and VIC. In both tidal spectra, it is dominant at southern hemisphere high-latitude regions from November to April. The second in amplitude among non-migrating components is SW3, having similar month-to-month variation in EsOR and VIC only in the southern hemisphere.

At low latitudes, DE2 and DE3 have the largest amplitudes in the non-migrating components of EsOR

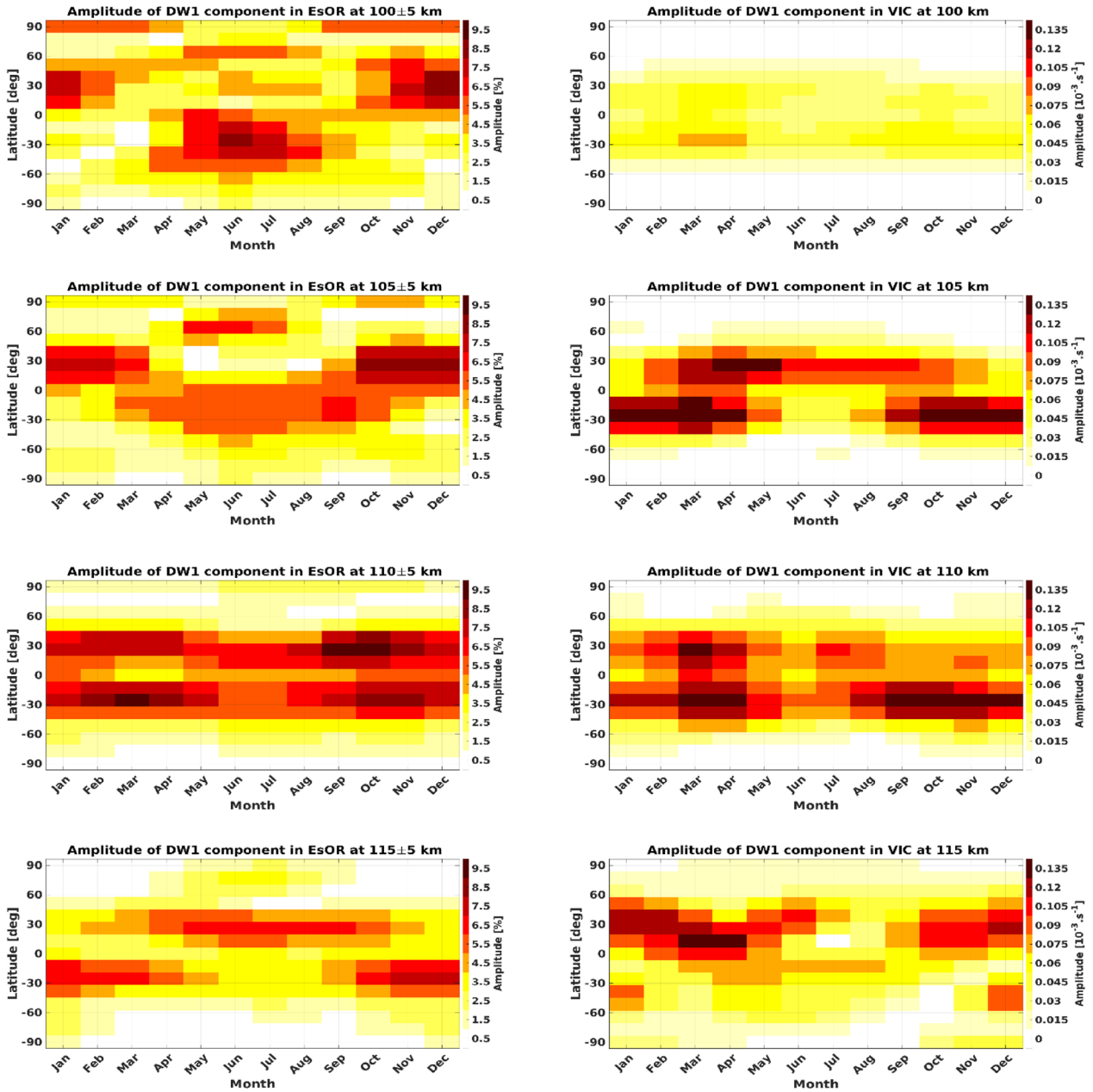

Fig. 5 Month-to-month amplitude variation of DW1 component of tides in EsOR (left column) and VIC (right column) at different altitudes

and VIC. DE3 component is dominant during July to September in VIC and EsOR tidal spectra. Around winter and summer solstice in low latitudes, DE2 component is maximum.

Considering only the latitudinal variation of tidal components, DE3 of EsOR and VIC are in good agreement; however, their monthly variations do not match perfectly. DE2 component of tides follows a similar seasonal distribution in EsOR and VIC at the latitude band of 30 ° south to 30 ° north.

Discussion

The results have shown that tidal components in EsOR are in agreement with those in VIC. In general, the consistency between tidal components in EsOR and VIC

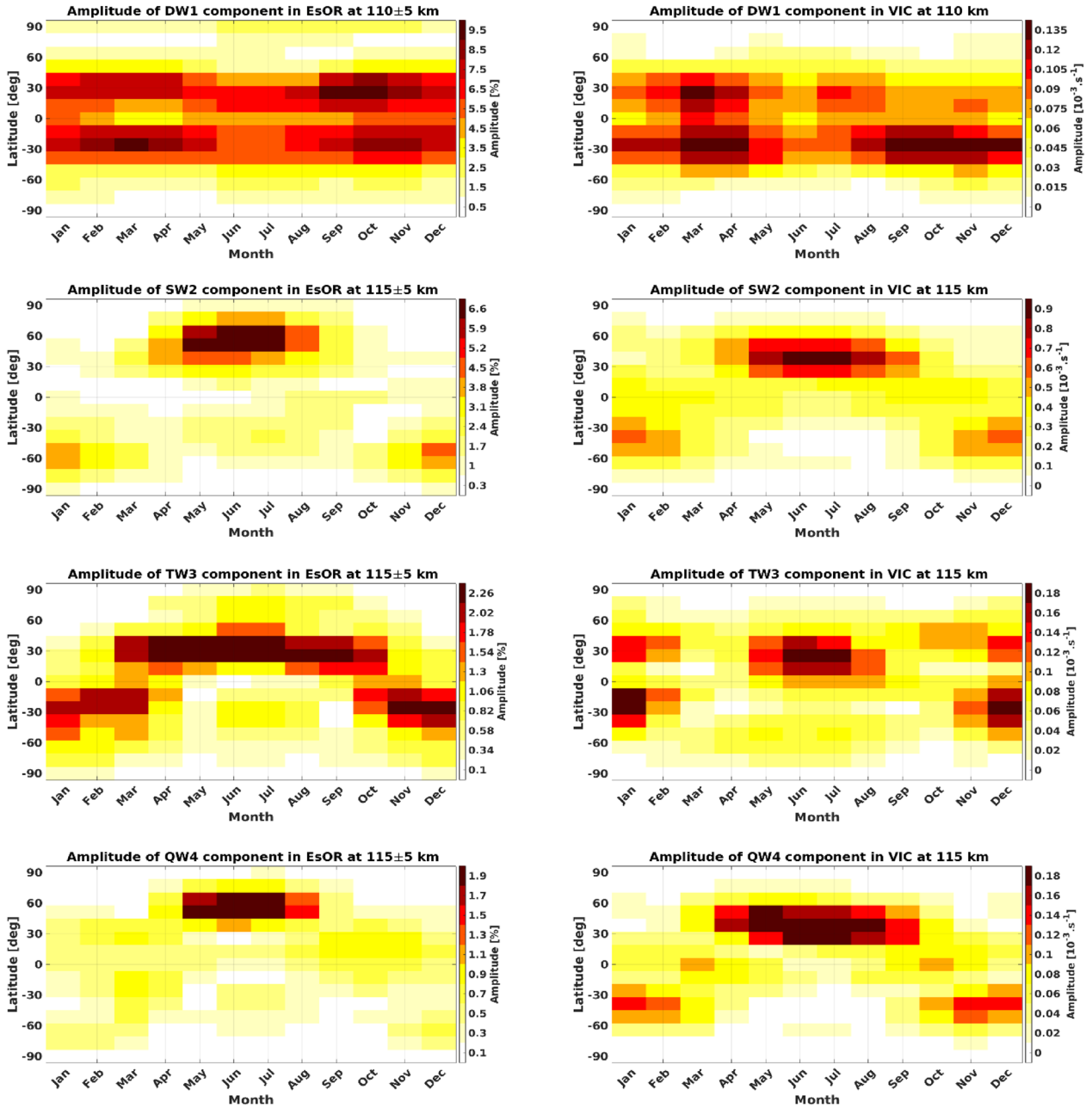

Fig. 6 Month-to-month amplitude variation of migrating components of tides in EsOR (left column) and VIC (right column)

confirms that wind shears generated by tides play a major role in Es layer formation.

According to Fig. 7, SW1 and SW3 components have the highest amplitudes among all non-migrating tidal components in EsOR. This can be explained by two possible mechanisms. First, SW1 and SW3 in EsOR could originate from corresponding tidal components in the neutral atmosphere, produced by nonlinear interaction of the SW2 and stationary planetary wave with zonal wavenumber 1 in that region (Miyoshi et al. 2017). Second, SW1 and SW3 in EsOR could be generated by stationary wave number 1 structure in the Earth's magnetic

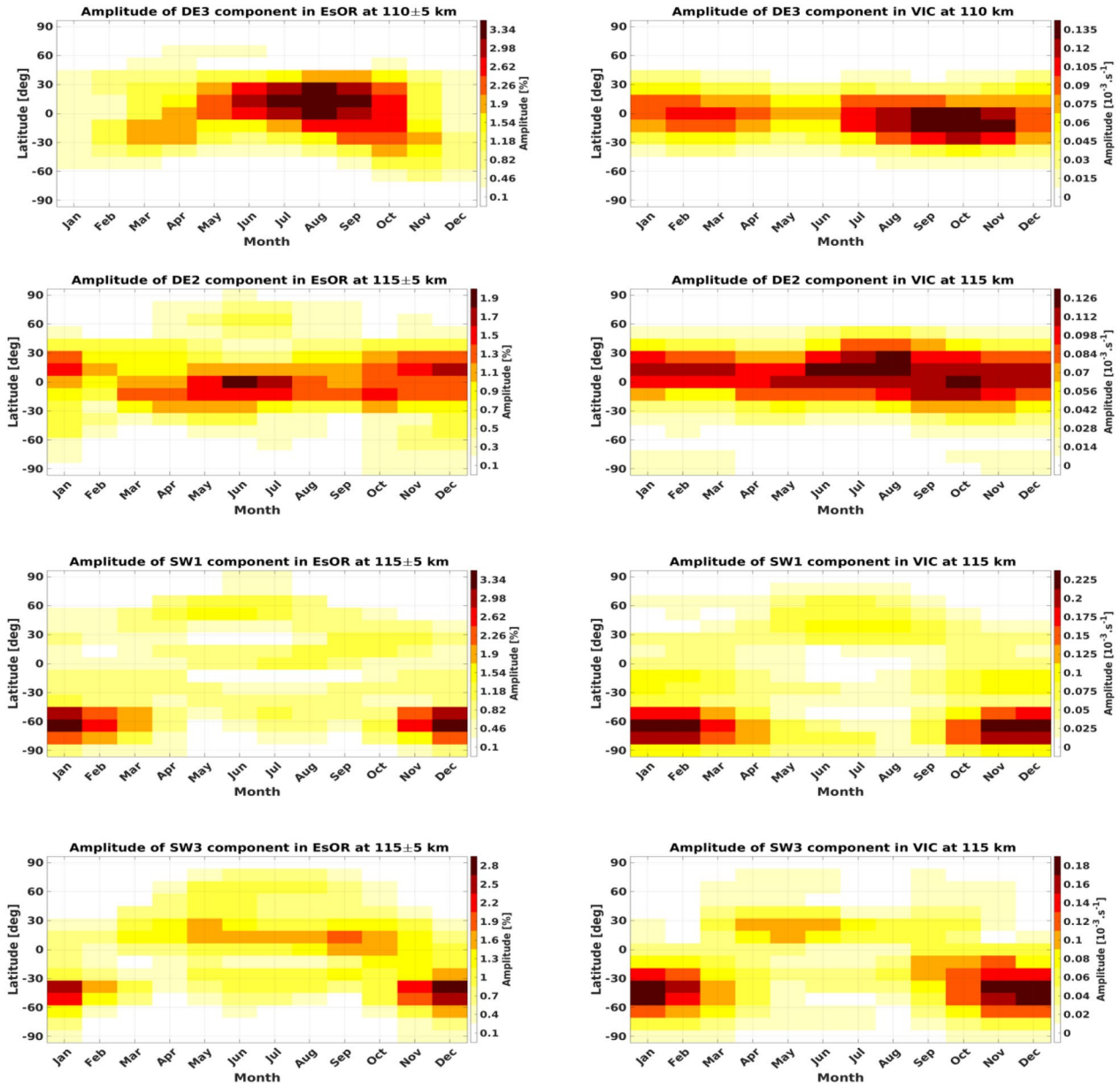

Fig. 7 Month-to-month amplitude variation of non-migrating components of tides in EsOR (left column) and VIC (right column)

field (**B**) and SW2 in the horizontal neutral wind velocity (**V**), because Es layers are formed by Lorentz force ($\mathbf{V} \times \mathbf{B}$). Seasonal variations of SW1 and SW3 components of VIC at different latitudes are presented in the top panel of Fig. 8. The middle panel shows the same, but for the zonal wind term in VIC ($\partial(\frac{r\cos I}{1+r^2}U)/\partial z$). The agreement of these two confirms that the vertical shear of the zonal wind has the primary role in VIC. The bottom panel of Fig. 8 shows the zonal wind term in VIC, but magnetic field-related terms (r and I) were replaced by their zonal mean to remove the effect of zonal asymmetry in the Earth's magnetic field. Comparing the two bottom panels, we conclude that zonal asymmetry of the Earth's magnetic field does not play a major role in the SW1 and SW3 components of VIC and consequently Es layer formation. Therefore, SW1 and SW3, seen in EsOR,

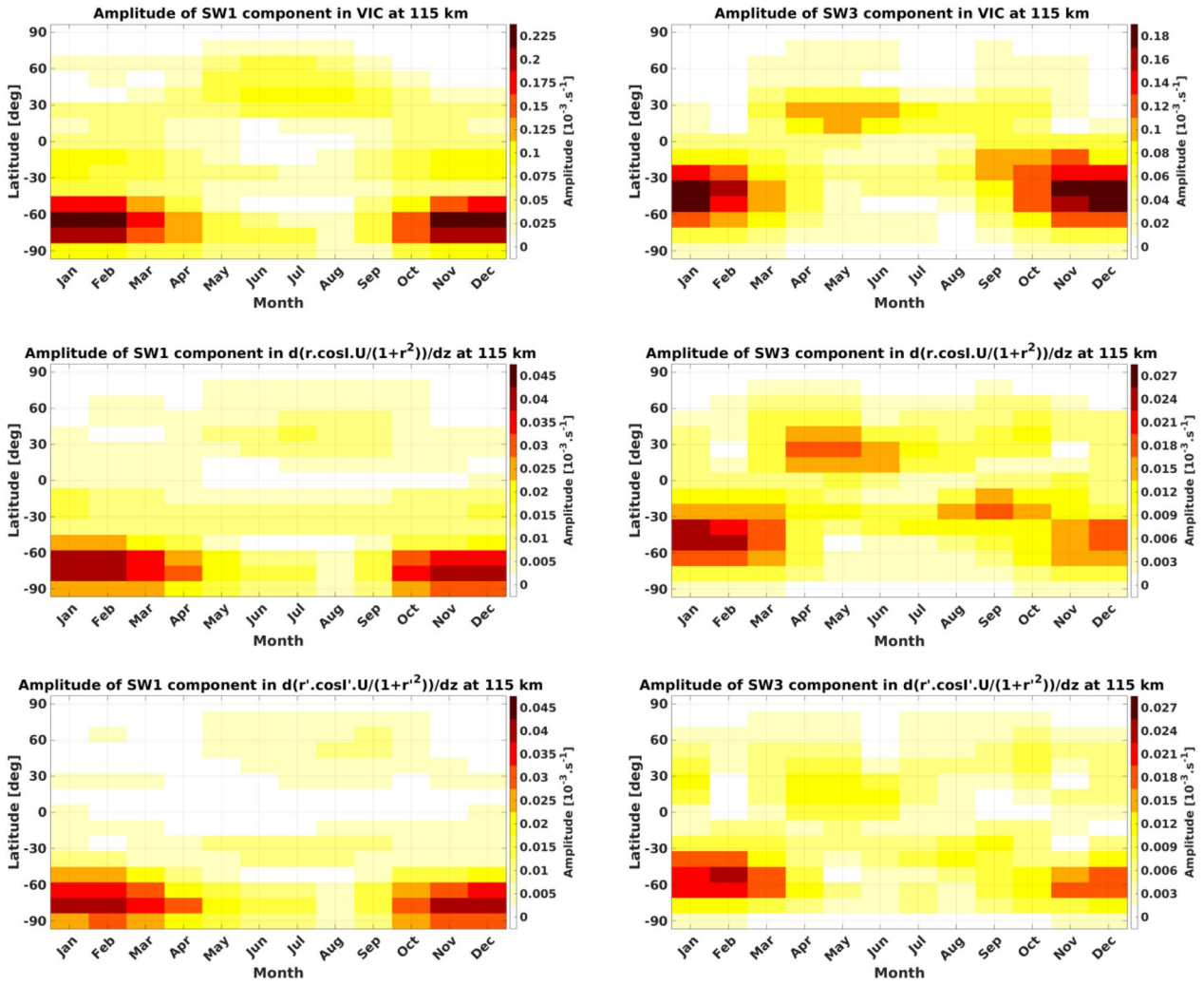

Fig. 8 Month-to-month amplitude variation of SW1 (left column) and SW3 (right column) components of VIC (first row), zonal wind term in VIC (second row) and the zonal wind term VIC without the effect of magnetic field zonal asymmetry (third row) at different altitudes

are due to the presence of those components in the neutral atmosphere.

The results of this research bring up questions that can be answered in future studies. Comparison of VIC and EsOR tidal components presented in the current paper was based on solar tides. Since GAIA does not include mechanisms to produce lunar tides, further studies using wind models, including lunar tides, could be done to examine lunar tidal components of VIC and their influence on Es layer formation. Moreover, based on Fig. 5, seasonal and latitudinal variations of EsOR tidal components match those in VIC at higher altitudes. Therefore, further research using other wind model simulations is needed to see whether the agreement in tidal components of VIC and EsOR would improve.

Conclusions

This study has examined the role of atmospheric tides in Es layer formation using RO data of FORMOSAT-3/COSMIC and GAIA model simulations. Tidal analysis has been performed on EsOR and VIC to derive the amplitude of different tidal components. Seasonal variations of migrating and non-migrating tidal components of EsOR and VIC were also studied at different latitudes. The main results are as follows:

1- Analyzing 11-year Es, a semidiurnal solar and lunar tidal pattern is visible in the mid-latitude EsOR. This confirms previous studies (e.g., Arras et al. 2009; Matsushita 1962) and provides a comprehensive picture of lunar tidal signature in Es occurrence rate, using global RO data.

2- Performing spectral analysis on Es data, a qualitative difference between solar and lunar tidal signature in EsOR is evident. Solar tides include both migrating and non-migrating components, while lunar tides show only the dominance of semidiurnal migrating component at mid-latitude.

3- Deriving neutral winds from GAIA model simulation, comparisons between vertical ion convergence induced by neutral winds and Es occurrence rate are made. Among all different tidal components, the amplitudes of SW2, DW1, DE2 and SW1 in EsOR show seasonal and latitudinal variations similar to those in the corresponding components of VIC. These agreements suggest that tidal components in EsOR are primarily associated with atmospheric tides.

4- SW1 and SW3 are the most dominant non-migrating tidal components of EsOR in southern hemisphere high latitudes. SW1 and SW3 components in EsOR are likely generated by the corresponding tides in neutral atmosphere. Our numerical experiments suggest that the zonal asymmetry of the Earth's magnetic field does not play a major role in producing SW1 and SW3 in EsOR.

Appendix 1

EsOR altitude–lunar local time cross-sections during mid-latitude local summers at night and day sides separately.

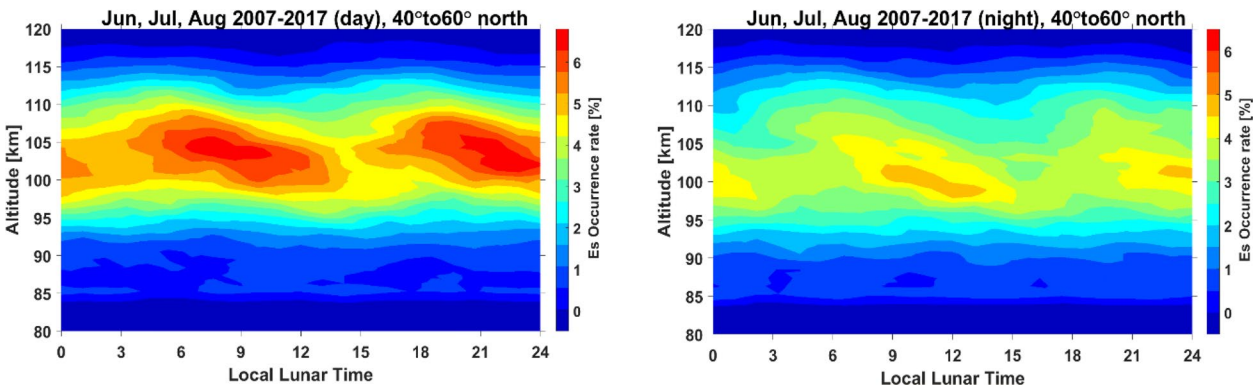

Figure a Mid-latitude EsOR variations during northern hemisphere summer with lunar local time at day (left) and night (right).

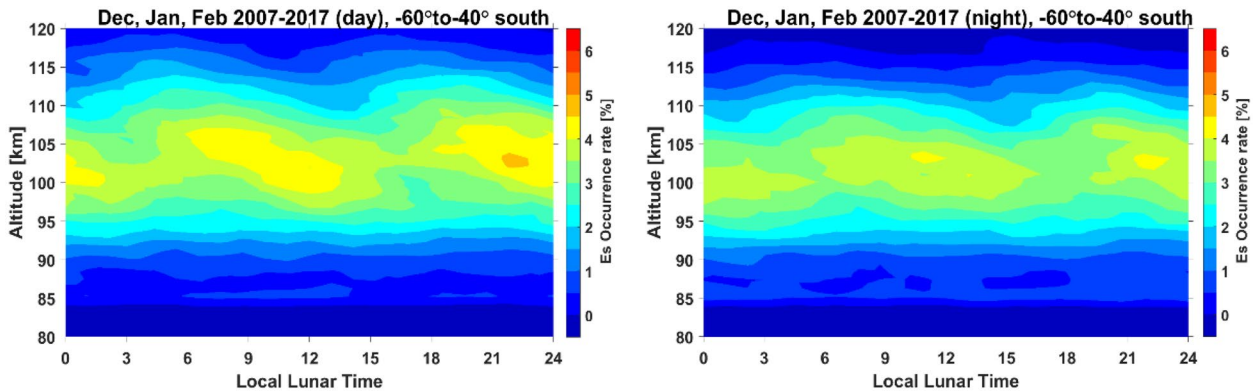

Figure b Mid-latitude EsOR variations during southern hemisphere summer with lunar local time at day (left) and night (right).

Abbreviations

GAIA	Ground-to-topside model of Atmosphere and Ionosphere for Aeronomy
Es	Sporadic E
EsOR	Es occurrence rate
VIC	Vertical ion convergence
RO	Radio occultation
GPS	Global Positioning System
SAA	South Atlantic Anomaly
FORMOSAT–3/COSMIC	FORMOsa SATellite mission-3/Constellation Observing System for Meteorology, Ionosphere and Climate

Acknowledgements
CA acknowledges support by the DFG Priority Program DynamicEarth, SPP 1788 under grant AR953/1-2.

Author contributions
SS did the data analysis and wrote the paper. YY discussed the results and contributed to revise the paper. CA extracted the Es signatures from the SNR of the GPS signal. YM and HS performed GAIA simulations and the interpretation of the GAIA results. All authors read and approved the final manuscript.

Funding
Open Access funding enabled and organized by Projekt DEAL. This work was supported in part by JSPS and DFG (Grant YA-574-3-1) under the Joint Research Projects LEAD with DFG (JRPs-LEAD with DFG).

Availability of data and materials
Raw data of GAIA are available at: https://gaia-web.nict.go.jp/data_e.html. The level 1b atmPhs radio occultation data from the F3/C mission are available at COSMIC Data Analysis and Archive Center: https://www.cosmic.ucar.edu/what-we-do/cosmic-1/data/.

Declarations

Competing interests
The authors declare that they have no competing interests.

Author details
[1]GFZ German Research Centre for Geosciences, Faculty of Science University of Potsdam, Potsdam, Germany. [2]GFZ German Research Centre for Geosciences, Potsdam, Germany. [3]Yasunobu Miyoshi Kyushu University, Fukuoka, Japan. [4]National Institute of Information and Communications Technology, Tokyo, Japan.

Received: 1 November 2021 Accepted: 29 April 2022
Published: 7 June 2022

References

Andoh S, Saito A, Shinagawa H, Ejiri MK (2020) First simulations of day-to-day variability of mid-latitude sporadic E layer structures. Earth Planets Space 72(1):1–9. https://doi.org/10.1186/s40623-020-01299-8

Arras C (2010) A global survey of sporadic E layers based on GPS Radio occultations by CHAMP, GRACE and FORMOSAT-3/COSMIC (Doctoral dissertation, Deutsches GeoForschungsZentrum GFZ Potsdam). Doi: https://doi.org/10.2312/GFZ.b103-10097.

Arras C, Wickert J (2018) Estimation of ionospheric sporadic E intensities from GPS radio occultation measurements. J Atmos Solar Terr Phys 171:60–63. https://doi.org/10.1016/j.jastp.2017.08.006

Arras C, Wickert J, Beyerle G, Heise S, Schmidt T, Jacobi C (2008) A global climatology of ionospheric irregularities derived from GPS radio occultation. Geophys Res Lett. https://doi.org/10.1029/2008GL034158

Arras C, Jacobi C, Wickert J (2009) Semidiurnal tidal signature in sporadic E occurrence rates derived from GPS radio occultation measurements at higher mid-latitudes. Ann Geophys 27(6):2555–2563. https://doi.org/10.5194/angeo-27-2555-2009

Arras C, Jacobi C, Wickert J, Heise S, Schmidt T (2010) Sporadic E signatures revealed from multi-satellite radio occultation measurements. Adv Radio Sci 8:225–230. https://doi.org/10.5194/ars-8-225-2010

Axford W, Cunnold D (1966) The wind-shear theory of temperate zone sporadic E. Radio Sci 1(2):191–197. https://doi.org/10.1002/rds196612191

Christakis N, Haldoupis C, Zhou Q, Meek C (2009) Seasonal variability and descent of mid-latitude sporadic E layers at Arecibo. Ann Geophys 27(3):923–931. https://doi.org/10.5194/angeo-27-923-2009

Chu Y-H, Wang C, Wu K, Chen K, Tzeng K, Su C-L, Feng W, Plane J (2014) Morphology of sporadic E layer retrieved from COSMIC GPS radio occultation measurements: wind shear theory examination. J Geophys Res Space Phys 119(3):2117–2136. https://doi.org/10.1002/2013JA019437

Emmert JT, Drob DP, Shepherd GG, Hernandez G, Jarvis MJ, Meriwether JW, Niciejewski RJ, Sipler DP, Tepley CA (2008) DWM07 global empirical model of upper thermospheric storm-induced disturbance winds. J Geophys Res 113:A11319. https://doi.org/10.1029/2008JA013541.

Finlay CC, Maus S, Beggan C, Bondar T, Chambodut A, Chernova T, Chulliat A, Golovkov V, Hamilton B, Hamoudi M (2010) International geomagnetic reference field: the eleventh generation. Geophys J Int 183(3):1216–1230. https://doi.org/10.1111/j.1365-246X.2010.04804.x

Forbes J, Zhang X, Palo S, Russell J, Mertens C, Mlynczak M (2008) Tidal variability in the ionospheric dynamo region. J Geophys Res. https://doi.org/10.1029/2007JA012737

Fytterer T, Arras C, Jacobi C (2013) Terdiurnal signatures in sporadic E layers at mid-latitudes. Adv Radio Sci 11(YSA):333–339. https://doi.org/10.5194/ars-11-333-2013

Fytterer T, Arras C, Hoffmann P, Jacobi C (2014) Global distribution of the migrating terdiurnal tide seen in sporadic E occurrence frequencies obtained from GPS radio occultations. Earth Planets Space 66(1):1–9. https://doi.org/10.1186/1880-5981-66-79

Haldoupis C (2011) A tutorial review on sporadic E layers. In: Mangalathayil AA, Dora P (eds) Aeronomy of the earth's atmosphere and ionosphere. Springer, Dordrecht, pp 381–394

Haldoupis C (2012) Mid-latitude sporadic E. A typical paradigm of atmosphere-ionosphere coupling. Space Sci Rev 168(1):441–461. https://doi.org/10.1007/s11214-011-9786-8

Haldoupis C, Pancheva D (2002) Planetary waves and mid-latitude sporadic E layers: strong experimental evidence for a close relationship. J Geophys Res. https://doi.org/10.1029/2001JA000212

Haldoupis C, Pancheva D (2006) Terdiurnal tide-like variability in sporadic E layers. J Geophys Res. https://doi.org/10.1029/2005JA011522

Haldoupis C, Pancheva D, Mitchell N (2004) A study of tidal and planetary wave periodicities present in mid-latitude sporadic E layers. J Geophys Res. https://doi.org/10.1029/2003JA010253

Haldoupis C, Pancheva D, Singer W, Meek C, MacDougall J (2007) An explanation for the seasonal dependence of mid-latitude sporadic E layers. J Geophys Res. https://doi.org/10.1029/2007JA012322

Igarashi K, Nakamura M, Wilkinson P, Wu J, Pavelyev A, Wickert J (2001) Global sounding of sporadic E layers by the GPS/MET radio occultation experiment. J Atmos Solar Terr Phys 63(18):1973–1980. https://doi.org/10.1016/S1364-6826(01)00063-3

Jacobi C, Arras C, Geißler C, Lilienthal F (2019) Quarterdiurnal signature in sporadic E occurrence rates and comparison with neutral wind shear. Ann Geophys 37(3):273–288. https://doi.org/10.5194/angeo-37-273-2019

Jin H, Miyoshi Y, Fujiwara H, Shinagawa H, Terada K, Terada N, Ishii M, Otsuka Y, Saito A (2011) Vertical connection from the tropospheric activities to the ionospheric longitudinal structure simulated by a new Earth's whole atmosphere-ionosphere coupled model. J Geophys Res. https://doi.org/10.1029/2010JA015925

Liu H, Sun YY, Miyoshi Y, Jin H (2017) ENSO effects on MLT diurnal tides: a 21 year reanalysis data-driven GAIA model simulation. J Geophys Res Space Phys 122(5):5539–5549. https://doi.org/10.1002/2017JA024011

Liu Y, Zhou C, Tang Q, Li Z, Song Y, Qing H, Ni B, Zhao Z (2018) The seasonal distribution of sporadic E layers observed from radio occultation measurements and its relation with wind shear measured by TIMED/TIDI. Adv Space Res 62(2):426–439. https://doi.org/10.1016/j.asr.2018.04.026

Liu Z, Fang H, Yue X, Lyu H (2021) Wavenumber-4 patterns of the sporadic E over the middle-and low-latitudes. J Geophys Res 126(8):e2021JA029238. https://doi.org/10.1029/2021JA029238
Lühr H, Manoj C (2013) The complete spectrum of the equatorial electrojet related to solar tides: CHAMP observations. Ann Geophys 31(8):1315–1331. https://doi.org/10.5194/angeo-31-1315-2013
Macleod MA (1966) Sporadic E theory. I. Collision-geomagnetic equilibrium. J Atmos Sci 23(1):96–109. https://doi.org/10.1175/1520-0469(1966)023
Mathews J (1998) Sporadic E: current views and recent progress. J Atmos Solar Terr Phys 60(4):413–435. https://doi.org/10.1016/S1364-6826(97)00043-6
Mathews JD, Bekeny F (1979) Upper atmosphere tides and the vertical motion of ionospheric sporadic layers at Arecibo. J Geophys Res Space Phys 84(A6):2743–2750. https://doi.org/10.1029/JA084iA06p02743
Matsushita S (1952) Semidiurnal lunar variations in the sporadic-E. J Geomagn Geoelectr 4(1):39–40. https://doi.org/10.5636/jgg.4.39
Matsushita S (1957) Lunar effects on the equatorial Es. J Atmos Terr Phys 10(3):163–165. https://doi.org/10.1016/0021-9169(57)90097-1
Matsushita S (1962) Lunar tidal variations of sporadic E. In: Matsushita S (ed) Ionospheric sporadic. Elsevier, Amsterdam, pp 194–214. https://doi.org/10.1016/B978-0-08-009744-2.50021-7
Matsushita S (1967) Lunar tides in the ionosphere. In: Bartels J (ed) Geophysik III/Geophysics III. Springer, pp 547–602. https://doi.org/10.1007/978-3-642-46082-1_2
Miyoshi Y, Pancheva D, Mukhtarov P, Jin H, Fujiwara H, Shinagawa H (2017) Excitation mechanism of non-migrating tides. J Atmos Solar Terr Phys 156:24–36. https://doi.org/10.1016/j.jastp.2017.02.012
Oikonomou C, Haralambous H, Haldoupis C, Meek C (2014) Sporadic E tidal variabilities and characteristics observed with the Cyprus Digisonde. J Atmos Solar Terr Phys 119:173–183. https://doi.org/10.1016/j.jastp.2014.07.014
Pancheva D, Haldoupis C, Meek C, Manson A, Mitchell N (2003) Evidence of a role for modulated atmospheric tides in the dependence of sporadic E layers on planetary waves. J Geophys Res. https://doi.org/10.1029/2002JA009788
Qiu L, Zuo X, Yu T, Sun Y, Qi Y (2019) Comparison of global morphologies of vertical ion convergence and sporadic E occurrence rate. Adv Space Res 63(11):3606–3611. https://doi.org/10.1016/j.asr.2019.02.024
Richmond AD (1995) Ionospheric electrodynamics. Handbook of atmospheric electrodynamics, 1
Shinagawa H, Miyoshi Y, Jin H, Fujiwara H (2017) Global distribution of neutral wind shear associated with sporadic E layers derived from GAIA. J Geophys Res Space Physics 122(4):4450–4465. https://doi.org/10.1002/2016JA023778
Stening RJ (1999) The lunar tide in sporadic E. Ann Geophys 17(10):1344–1351. https://doi.org/10.1007/s00585-999-1344-2
Tarpley J, Matsushita S (1971) The lunar tide in fbEs. Radio Sci 6(2):191–196. https://doi.org/10.1029/RS006i002p00191
Tarpley J, Matsushita S (1972) Lunar influences on sporadic E. Radio Sci 7(3):411–416. https://doi.org/10.1029/RS007i003p00411
Voiculescu M, Haldoupis C, Schlegel K (1999) Evidence for planetary wave effects on mid-latitude backscatter and sporadic E layer occurrence. Geophys Res Lett 26(8):1105–1108. https://doi.org/10.1029/1999GL900172
Whitehead J (1961) The formation of the sporadic-E layer in the temperate zones. J Atmos Terr Phys 20(1):49–58. https://doi.org/10.1016/0021-9169(61)90097-6
Whitehead J (1970) Production and prediction of sporadic E. Rev Geophys 8(1):65–144. https://doi.org/10.1029/RG008i001p00065
Whitehead J (1989) Recent work on mid-latitude and equatorial sporadic-E. J Atmos Terr Phys 51(5):401–424. https://doi.org/10.1016/0021-9169(89)90122-0
Wu DL, Ao CO, Hajj GA, De La Torre JM, Mannucci AJ (2005) Sporadic E morphology from GPS-CHAMP radio occultation. J Geophys Res. https://doi.org/10.1029/2004JA010701
Yamazaki Y, Arras C, Andoh S, Miyoshi Y, Shinagawa H, Harding BJ, Englert CR, Immel TJ, Sobhkhiz-Miandehi S, Stolle C (2022) Examining the wind shear theory of sporadic E with ICON/MIGHTI winds and COSMIC-2 radio occultation data. Geophys Res Lett. https://doi.org/10.1029/2021GL096202
Yeh WH, Liu JY, Huang CY, Chen SP (2014) Explanation of the sporadic-E layer formation by comparing FORMOSAT-3/COSMIC data with meteor and wind shear information. J Geophys Res 119(8):4568–4579. https://doi.org/10.1002/2013JD020798

Publisher's Note